The emergent Yo-yo movement of nuclei driven by collective cytoskeletal remodeling in pseudo-synchronous mitotic cycles

Zhiyi Lv[1], Jan Rosenbaum[2], Xiaozhu Zhang[3], Stephan Mohr[4], Helen Preiß[5], Sebastian Kruss[5], Karen Alim[4], Timo Aspelmeier[2], Jörg Großhans[1]

1. Institut für Entwicklungsbiochemie, Universitätsmedizin, Georg-August-Universität Göttingen, Germany.
2. Institut für Mathematische Stochastik, Georg-August-Universität Göttingen, Germany.
3. Chair for Network Dynamics, Institute for Theoretical Physics and Center for Advancing Electronics Dresden (cfaed), Cluster of Excellence Physics of Life, TU Dresden, 01062 Dresden,
4. Germany Max Planck Institute for Dynamics and Self-Organization, Göttingen, Germany,
5. Institut für Physikalische Chemie, Georg-August-Universität Göttingen, Germany

corresponding author:
Zhiyi Lv
lv.zhiyi@med.uni-goettingen.de
Jörg Großhans
jgrossh@gwdg.de

Classification: Biological science, Developmental Biology, Systems Biology.

Abstract:
Many aspects in tissue morphogenesis are attributed to the collective behavior of the participating cells. Yet, the mechanism for emergence of dynamic tissue behavior is not understood completely. Here we report the "yo-yo"-like nuclear drift movement in *Drosophila* syncytial embryo displays typical emergent feature of collective behavior, which is associated with pseudo-synchronous nuclear division cycle. We uncover the direct correlation between the degree of asynchrony of mitosis and the nuclear collective movement. Based on experimental manipulations and numerical simulations, we find the ensemble of spindle elongation, rather than a nucleus' own spindle, is the main driving force for its drift movement. The cortical F-actin effectively acts as a viscoelastic material dampening the drift movement and ensuring the nuclei return to the original positions. Our study provides insights into how the interactions between cytoskeleton as individual elements leads to collective movement of the nuclear array on a macroscopic scale.

Keywords: syncytium, nuclear array, cortex, microtubule, F-actin, formin, Dia, network, emergent behavior, ELMO, flow, biomechanics

Introduction

Collective behaviors emerge from many interacting individuals in the absence of central coordination and supervision. Birds flocks, fish schools, as well as bacterial colonies exhibit spontaneous synchronization and many other complex dynamic functional patterns originating from simple local interaction rules (1-3). Within a single organism, self-organized collective behaviors are an inseparable part in maintaining its basic biological functions by efficiently driving numerous complex biological processes without external regulations such as neural activation in brain (4-6) and morphogenesis during embryonic development (7, 8). On subcellular scale, actin and microtubules form collective motion in the presence of motor proteins and ATP (9-11). Yet, despite the ubiquitousness and the significance of emergent collective behavior in biology, our knowledge of the fundamental mechanism of functional collective behaviors are very limited. The major obstacle lies in the typically extremely complex interactions between the individuals in most biological collective behaviors. However, in syncytial insect embryo only direct cytoskeletal interactions exist, owing to the lack of membranes separating the nuclei, which enables dissecting and understanding how the interactions of individuals drive the formation of emergent features at tissue level.

To obtain insights into the molecular mechanism leading to the emergence of a collective flow movement, we study the dynamics of nuclear array in *Drosophila* syncytial blastoderm, where the direct interactions between individuals lead to at least three features of emergent collective behavior observed at tissue level. Firstly, the nuclei divide synchronously to their immediate neighbors but asynchronously to more distant nuclei. This leads to a wave front of mitosis sweeping over the embryo (12, 13). Secondly, the nuclei arrange in an ordered array in interphase following disturbance during nuclear division. Ordering involves

interactions by the microtubule asters but also with F-actin at the cortex (14, 15). Thirdly, the nuclei and the cytoplasm undergo stereotypic flow movements following the mitotic wave, which is reminiscent of the toy “yo-yo”. This arises the questions: is there any physiological function of this flow? How does the flow emerge and what are the underlying driving forces?

The large scale collective movements are driven by active elements of the cytoskeleton. For example, kinesin-1 and microtubules drive the cytoplasmic streaming during *Drosophila* oogenesis (16). The cytoplasmic streaming in plant and algae is driven by myosin moving on F-actin (17, 18). Apical constriction mediated by actomyosin can generate the cytoplasmic flow, which compels nuclear spreading in *Drosophila* pre-blastoderm (19) and cell elongation in gastrulation (20).

In *Drosophila* syncytial blastoderm, the nuclei and their associated centrosomes and microtubule asters form an extended two-dimensional array (14). The dynamics of this array is dominated by two different interactions (21). Lateral interactions between the neighbor nuclei and centrosomes are mediated by microtubules and the associated motor proteins. The interactions between centrosomes and actin cortex constitute the cortical interactions. How these interactions lead to the stereotypic nuclear movement is unknow.

Beside the force generating mechanism, the material properties of the embryos (22-24) may influence the movement of the nuclei. The actin cytoskeleton inhibits short time-scale movements (21) and promotes ordering of the nuclear array (14). The actin cortex may act as a viscoelastic medium, to which the centrosomes and their associated nuclei are connected.

Here we found that the nuclear movement was isotropic for individual spindles but anisotropic for the collective flow over several nuclear diameters away from the mitotic wave front and back to the original position slightly later. We comprehensively quantified nuclear trajectories in wild type and mutant embryos and modelled the process by computational simulation. In this way, we uncovered that the ensemble of spindle elongation, rather than a nucleus’ own spindle, is the main driving force for its drift movement. In addition, we defined a function of cortical F-actin for the apparent viscoelastic material properties to restore the nuclear position.

Results

Long mitotic spindles and distance between daughter nuclei require pseudo-synchronous nuclear cycles

To elucidate the mechanisms that arise the emergent features of nuclear array dynamics in *Drosophila* syncytial cleavage cycle, we first documented the nuclear separation profile. We found that in mitosis the daughter nuclei are separated by an overshooting spindle, which

pushes apart the daughter nuclei more than the average inter-nuclear distance (Fig. 1A, B). With every division during the syncytial blastoderm (nuclear cycles NC 10–13), the nuclear density at the cortex doubles (Supp. Data Fig. S1). The nuclei divide slightly asynchronous especially during the last syncytial division in NC13 with a time lag of up to minutes, which is easily visible as a mitotic wave front sweeping over the embryo (Fig. 1C, Supp. Data Fig. S2A, B, Movie 1). The function and the consequences of this pseudo-synchrony are unknown. Given the increase of asynchrony with nuclear density, we speculated that spindle overshooting with nuclear crowding may pose a problem for synchronous divisions.

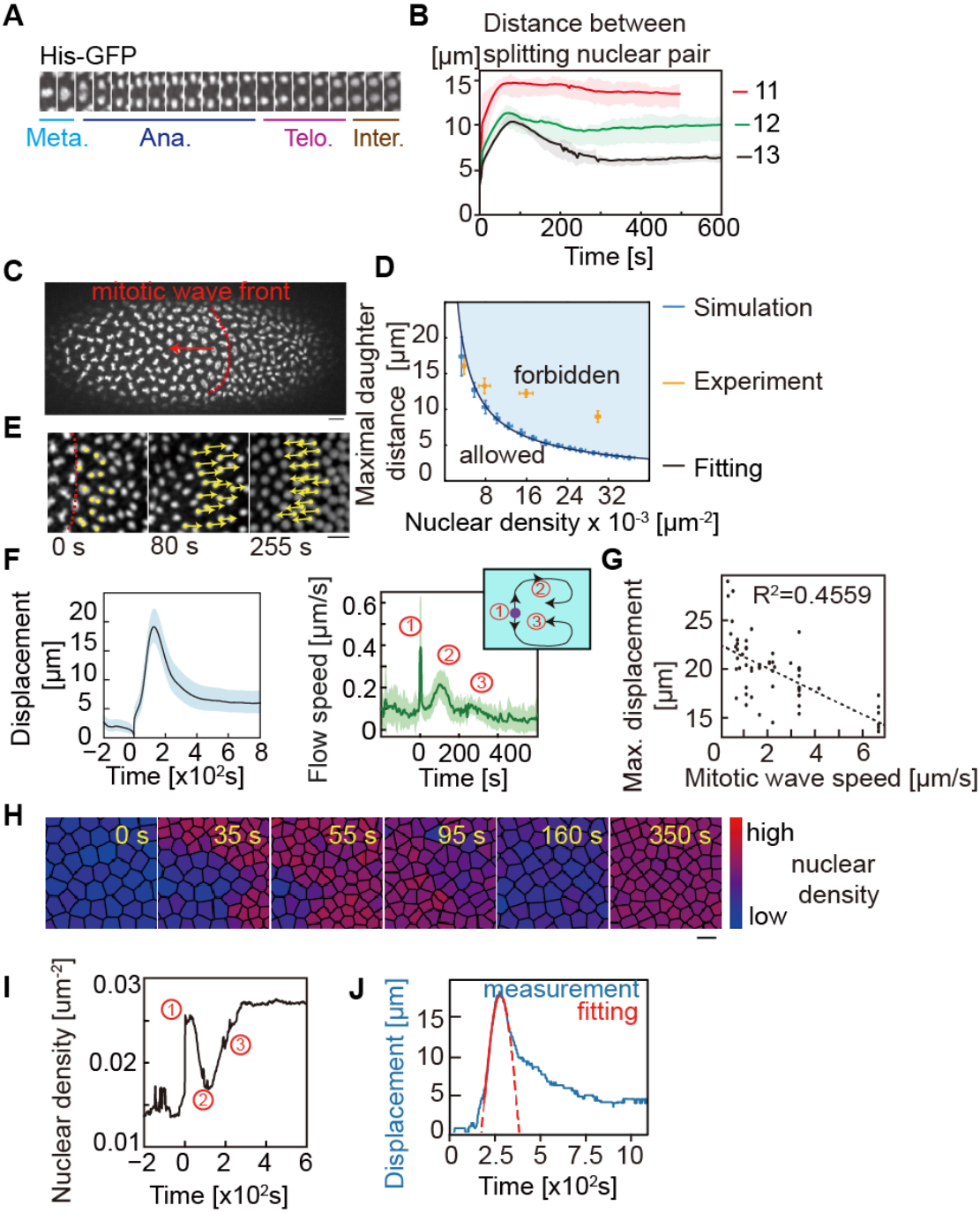

Figure 1. Quantitative assay for nuclear movement. (A)**,** Live image of an embryo during mitosis. The left half is in metaphase, the right half in anaphase. The dotted line in red indicates metaphase-anaphase

transition sweeping over the embryo from right to left as a wave front. (B), Spindle lengths/distances between daughter nuclei are plotted against the corresponding nuclear density. Data from simulation (blue) and measurements in embryos in NC11, NC12, NC13 and NC14 in haploids (orange) (n=15 spindles in each embryo and 3 embryos for each type). (C), Live images with nuclear labelling. Dotted line indicates the wave front of the metaphase-anaphase transition. Arrows in yellow indicate nuclear movement. (D), Time course of nuclear displacement with the position of the mother nucleus and nuclear speeds during metaphase-anaphase transition as a reference (t=0) (n=260 nuclei in one embryo). Insert is the schematic drawing of (1) chromosome segregation, (2) forth movement away and (3) back movement toward the mitotic wave front. (E), The maximal displacement plotted against the corresponding speed of the mitotic wave (n=50 embryos). (F), Image series with Voronoi maps with the mitotic wave front in images at 35 s and 55 s. Color code indicates nuclear density. (G), Time course of nuclear density with metaphase-anaphase transition at t=0. Numbers indicate the three stages of nuclear movement. (n=260 nuclei in one embryo). (H), A simple square function (red) was fitted to the forth and back movement around the maximal displacement. According to Hook's law an apparent spring constant ($1.5\pm0.02\times10^{-18}$ Nm^{-1}) was calculated (n=15 nuclei from 3 embryos). Data are mean±s.e.m. Scale bar: 10 μm.

To test this hypothesis, we simulated nuclear divisions within a limited area. We assigned each nucleus and mitotic spindles a protected area representing the entity in real embryos (Supp. Data Fig. S2B). After chromosome division, the daughter nuclei were pushed apart until reaching the protected area of a neighboring spindles/pair of daughter nuclei, thus assessing the maximal possible distance between daughter nuclei (maximal spindle length). We assumed synchronous divisions and symmetric spindles with isotropic orientations (Supp. Data Fig. S2C). Our simulations showed that the maximal spindle length decreased with an increase in nuclear number and thus marked the transition line between structurally allowed and forbidden regime of combinations of nuclear density and spindle length (Fig. 1D). Next, we measured the maximal distance between daughter nuclei and their corresponding nuclear densities in wild type embryos (Supp. Data Fig. S1). We also included data from haploid embryos, which undergo an extra nuclear division. Only the parameters of NC11 fell into the allowed area, whereas the parameters of NC12, NC13, and NC14 in haploids fell into the forbidden regime. This analysis indicated that a synchronous division with the observed spindle lengths was possible only in the early cycles but impossible in later cycles. Thus, pseudo-synchrony allows for the observed spindle length in NC12, NC13 and NC14 in haploid embryos.

Collective flow and density changes follow the mitotic wave front

The mitotic pseudo-synchrony and its corresponding wave front are associated with a stereotypic nuclear movement, which can be readily observed in time lapse movies (Fig. 1E, Supp. Data Movie 2). To obtain a precise description of the nuclear movements, we determined the trajectories of all nuclei within the field of view from time lapse recordings of fluorescently labeled nuclei. From the trajectories, we extracted time courses for displacements, velocities, and nuclear density (Fig. 1F, G). Every nucleus is assigned an

individual time axis with the splitting of daughter chromosomes (metaphase-anaphase transition) as reference time t=0.

Concerning displacement (Fig. 1F), the nuclei moved in average about 20 µm which corresponds to about 4–5 nuclear diameters away from the position of their mother nucleus at t=0. The maximal displacement was reached after about 2 min (Fig. 1F). Following maximal displacement, the nuclei then returned to almost their initial position. This movement resembles yo-yo ball, and hereafter we refer it as yo-yo movement. We calculated the speed of nuclear movement from the individual trajectories as the derivative of the trajectories. The averaged flow speed revealed three peaks (Fig. 1F, right panel). The first peak corresponds to the chromosome segregation in anaphase with about 0.4 µm/s. The second peak after about 1 to 2 min corresponds to the flow away from the mitotic wave front. The least pronounced, third peak corresponds to the return movement after about 4 min.

Asynchronicity of mitosis might be prerequisite for yo-yo flow. To test whether there is a correlation, we collected data from 50 embryos (Fig. S2A) for quantification of the speed of wave front and maximal displacement. Plotting corresponding parameter sets revealed a negative correlation (R^2=45%, Fig. 1G), which suggests a slow wave is associated with a large displacement.

As flow is linked to density changes, we next established spatial and temporal maps of nuclear density. Each nucleus was assigned an area and corresponding density according to Voronoi segmentation (Fig. 1H, Supp. Data Movie 3). In the case of synchronous divisions, the density would be expected to double at t=0 (metaphase anaphase transition) and remain constant throughout interphase. In contrast, but consistent with the observed nuclear flow, our measurements revealed a peculiar time of the density. Although initially doubling, the density dropped in telophase before finally reaching the doubled density again a few minutes later (Fig. 1F, G). Corresponding profiles for displacement and flows were detected in preceding nuclear cycles 11 and 12, although in a less pronounced manner (Supp. Data Fig. S4).

The forth and back movement of the nuclei is reminiscent of a spring. To obtain a phenomenological description of this behavior, we applied a simple mechanical model to the nuclear trajectories during the period of maximal displacement (Fig. 1H). By fitting a square function to the displacement curve, we obtained an apparent spring constant for each nucleus. The actual value of the apparent spring constant is not informative, since our model and assumptions are too simple. Friction is not included, for example. Yet, the apparent constant helps to compare experimental conditions and mutant phenotypes.

Isotropic individual behavior is associated with an anisotropic collective flow

Our analysis revealed a collective directional flow of the nuclear array. Yet the individual spindles are isotropically oriented. The axes between daughter nuclei are uniformly distributed over the angles against the anterior-posterior axis of the embryo (Fig. 2Aa–C). In contrast, the same nuclei almost unidirectionally moved along the embryonic axis a minute later, indicating an anisotropic behavior (Fig. 2A–C). The transition of isotropic individual to anisotropic collective behavior is strikingly obvious in the extreme cases of spindle orientation. In the case of a spindle oriented in parallel to the embryonic axis, one set of chromosomes segregated towards, whereas the daughter chromosomes moved away the wave front during anaphase. One minute later both nuclei moved away from the wave front (Fig. 2D). Similarly, in case of a perpendicular orientation of chromosome segregation, the movement during anaphase was perpendicular to the embryonic axis but along the axis a minute later during collective flow. (Fig. 2D).

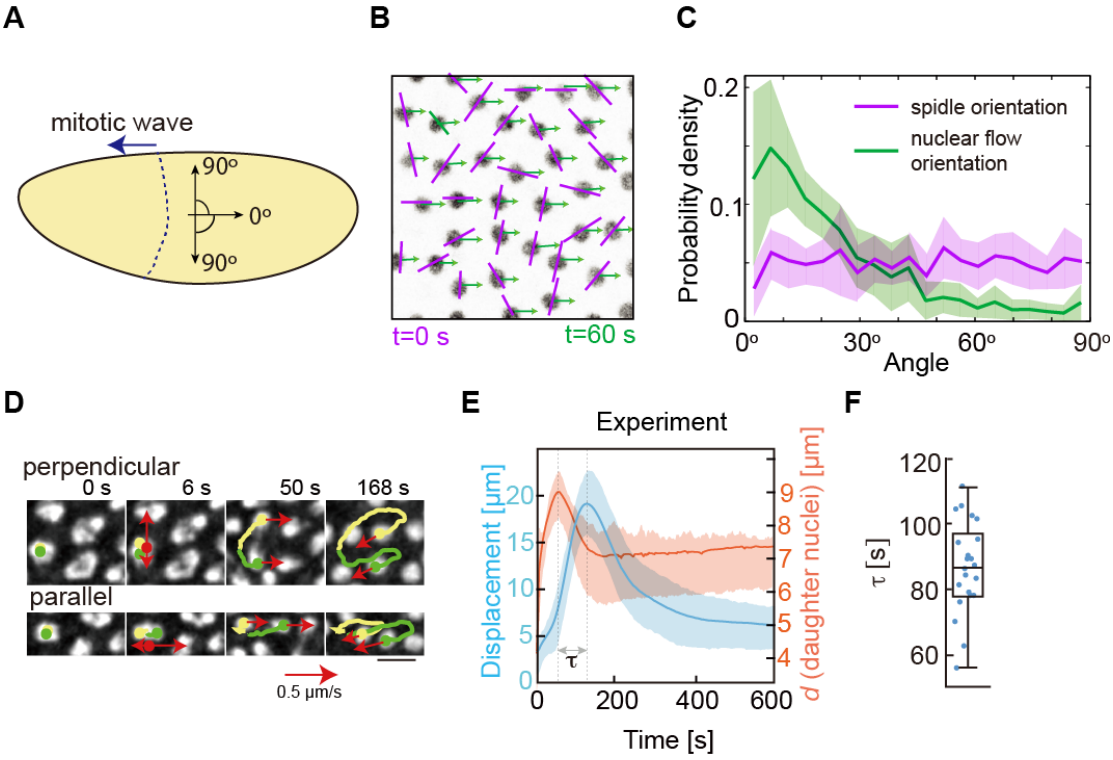

Figure 2. Emergence of collective nuclear movement. (A), Schematic drawing of an embryo with definition of angles. (B), Image from live imaging after mitosis. Orientations of the corresponding spindle at t=0 s and the directions of nuclear movement at t = 60 s are indicated by a magenta bar and green arrow, respectively. (C), Distribution of observed angles for spindle orientation at t=0 s and nuclear movement at t=60 s. (n=20 embryos including 6230 nuclei). (D), Image series with previous trajectories showing cases of perpendicular and parallel mitosis. (E), Time course of nuclear displacement (blue) and distance between corresponding daughter nuclei (orange). The time lag (τ) between maxima is indicated. (F), Distribution of the time lag (τ). Data are mean±s.e.m. Scale bar: 10 µm

The uncoupling of spindle behavior and nuclear behavior was seen not only in the orientation of the movements, but also in the time course of the two behaviors. The maximal displacement was reached only about 1.5 min after the maximal distance between

daughter nuclei (maximal spindle length) was reached (Fig. 2E), suggesting the maximal displacement was achieved when the nuclei are in telophase. These findings demonstrated that these two processes were mechanistically not directly linked at the individual level, since spindles were isotropically oriented and preceded the flow behavior.

During collective flow the nuclei may move as individuals characterized by neighbor exchanges. Alternatively nuclei may behave as an array, which would be indicated by fixed neighbor relationships. To distinguish these options, we labeled groups of cells before mitosis and followed them during the course of chromosome segregation and collective flow. We found that the nuclei moved as an array. The groups of nuclei did neither intersperse with unlabeled nuclei nor nuclei of the other groups indicating that neighbor relationships were maintained during mitosis and collective flow despite the movement over several nuclear diameters (Supp. Data Fig. S6F). In summary, our observations indicate that the nuclear layer phenomenologically behaves like an elastic sheet with fixed neighbor relationships.

Ensemble spindle elongation is the driving force for nuclear displacement

In the time-lapse image we found that telophasic nuclei were pushed away by the neighbor spindles which were in anaphase-B (Fig. 1C, Supp. Data Movie2). Although the spindle elongation and nuclear displacement are uncoupled at single element level, we speculated that the neighbor spindles drive nuclear yo-yo movements.

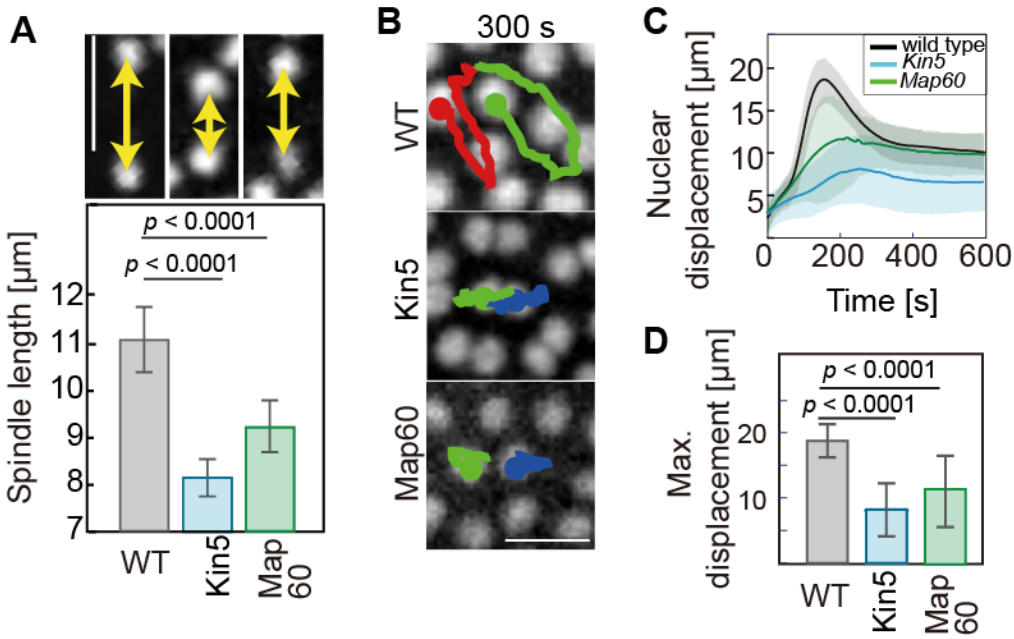

Figure 3. The ensemble of spindle elongation indirectly drives the nuclear movement. (A), The repulsive forces separating daughter nuclei are high in anaphase, followed by a drop in telophase. (B), The repulsive force map in a developing embryo. (C). Spindle length/distance between respective daughter nuclei in embryos partially depleted of Kinesin-5 and *Map60* mutants. (n=30 spindle in 3 embryos for each genotype). (D), Images from live image. The trajectories of two nuclei over 300 s were plotted into the last

images. (E, F), Quantification of nuclear trajectories for indicated genotypes. (E), Time course of nuclear displacement. (F), Maximal displacement. The Data are mean±s.e.m. Scale bar: 10 µm.

To test this hypothesis, we developed a method to reduce the spindle length globally, without hampering the nuclear separation. Spindle elongation in anaphase B requires the four-headed microtubule motor Kinesin 5, which can slide microtubules against each other (25). We employed embryos, in which endogenous Kinesin 5 was substituted by a version susceptible to TEV protease (26). We titrated the amount of TEV protease to achieve a partial depletion which still allowed completion of mitosis. Spindles in these embryos were short (Fig. 3C). The average maximal spindle length was 8 µm instead of 10 µm in wild type embryos. Complementary, we employed embryos from females homozygous for *Map60*, which also displayed short spindles(14) with an average length of 9 µm (Fig. 3A). Quantification of nuclear movement revealed a strongly reduced maximal displacement in both experimental conditions and thus a positive correlation of spindle length and maximal displacement (Fig. 3B, C, D). In summary, analysis of mutant embryos with shorter division distance support an overshooting of the mitotic spindle (pushing apart the daughter nuclei more than the average inter-nuclear distance) constitutes a major driving force for the nuclear movement thereafter.

Computational modeling of nuclear movement points to spindle length as a major driver of collective behavior

To gain an understanding for how the isotropic individual movements give rise to an anisotropic collective flow, we conducted numerical simulations. Starting from a theoretical model based on static nuclear interactions in interphase (15), we added a time axis for the interactions to account for the changes during mitosis. The model is based on active and passive forces (Supp. Data Fig. S5). Stochastic active forces repulse adjacent nuclei, thus resembling the sliding activity of motor proteins, e. g. Kinesin-5, on antiparallel aligned microtubules. In addition, a passive elastic force leads to repulsion accounting for the embedding of the nuclei into the cytoplasm and cytoskeleton. This may include the link of the nuclei to the cortex. Chromosome segregation is triggered at t=0 by a separation force acting between the daughter nuclei. The interaction forces are dynamic according to the mitotic stage and interphase (Supp. Data Fig. S5B). For example, the active force is low in anaphase, since astral microtubules prominently appear only in telo- and interphase. Similarly, the passive force increases in telo- and interphase as cortical actin increases during these stages. The segregation force decays in telo and interphase. Balancing the magnitude of passive and active forces over time, model simulation reproduced the experimentally observed stereotypic flow behavior (Fig. 4A. Data Movie 4).

Strikingly, the simulations reproduce other features of nuclear yo-yo movement. Firstly, maximal spindle length precedes maximal displacement with a time lag of 1.5 min (Fig. 4B, Fig. 2E). Secondly, the speed of the mitotic wave front is negatively correlated with the nuclear maximal displacement (Fig. 4C, Fig. 1A). Thirdly, the simulations resemble that the

force for separation of the daughter nuclei positively correlated with maximal distance between daughter nuclei and importantly with maximal displacement (Fig. 4D, Supp. Data Fig. S5D).

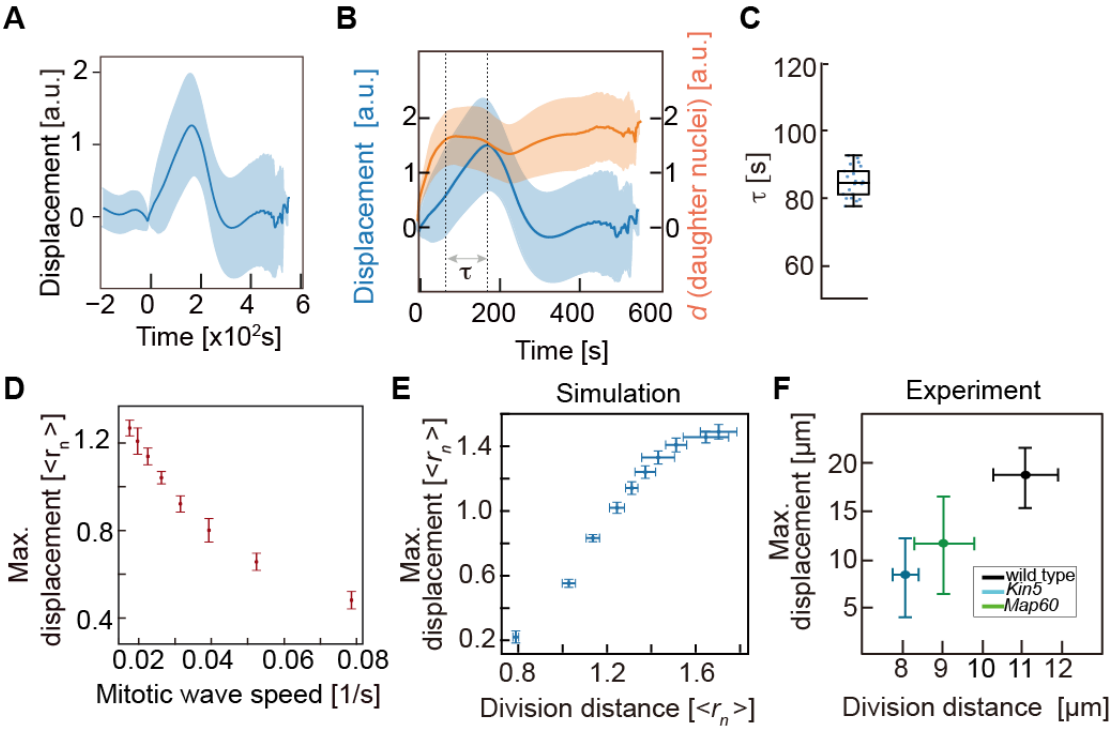

Figure 4. Numerical simulation of nuclear movement. (A), Time course of nuclear displacement (n=300 nuclei). (B), Time course of nuclear displacement (blue) and distance between corresponding daughter nuclei (orange). The time lag (τ) between maxima is indicated. (C), Distribution of the time lag (τ). (D), The negative correlation between maximal displacement and the corresponding speed of the mitotic wave. (E, F), Maximal displacement was plotted against corresponding division distance. Data from simulation (E) and experiment (F). Data are mean±s.e.m.

F-actin cortex is required for the return movement.

The simulation predicts a function of passive force in yo-yo movement. Cortical F-actin is a promising candidate. It has been previously reported that the nuclei are strongly attached to F-actin cortex (27). The actin cortex suppresses the fluctuation movements of centrosomes (21) and contributes to an ordered nuclear array in interphase (14). Cortical F-actin undergoes stereotypic remodeling during the course of nuclear cycles (28) (Fig. 5A, Supp. Data Fig. S6A). We quantified total F-actin with a Utrophin-GFP as a marker (29). We found that the signal dropped in mitosis, with lowest level during anaphase and steadily increased afterwards (Supp. Data Fig. S6A, B). Given the timing of this dynamics, it is conceivable that cortical actin plays an important part in controlling nuclear movement.

To test this conceivable function of the cortical F-actin, we employed two mutants to genetically interfere with the organization of the actin cortex (Supp. Data Fig. S6C). Firstly, we prevented the formation of actin caps with the mutant *ELMO* (21, 30). ELMO forms part

of an unconventional guanyl nucleotide exchange factor, which activates Rac signaling in a complex with Sponge/DOCK (31). *ELMO* mutants lack any actin caps and are characterized by a uniformly structured cortical F-actin (21) (Supp. Data Fig. S6C). Secondly, we employed *dia* mutants (32-34). Dia is a founding member of the formin family, which nucleate and polymerize linear actin filaments. *dia* mutants lack metaphase furrows but contain actin caps (32) (Supp. Data Fig. S6C).

We applied our quantitative assay to *ELMO* embryos. A strongly increased nuclear mobility was obvious in time lapse movies (Fig. 5B). Quantification of nuclear trajectories revealed a maximal nuclear displacement of 60 µm as compared to 20 µm in wild type embryos (Fig. 5D). In addition to the threefold increased displacement, we observed as a second phenotype that the nuclei did not return to their initial position in *ELMO* mutants (Fig. 5D, Supp. Data Fig. S6D). The impaired back movement indicates a loss of the spring-like behavior. Consistently, we calculated an almost 10-fold reduced spring constant at the turning point of the nuclear trajectories (Supp. Data Fig. S6E). A similar behavior and profiles were detected in NC12 of ELMO embryos (Supp. Data Fig. S6G, H).

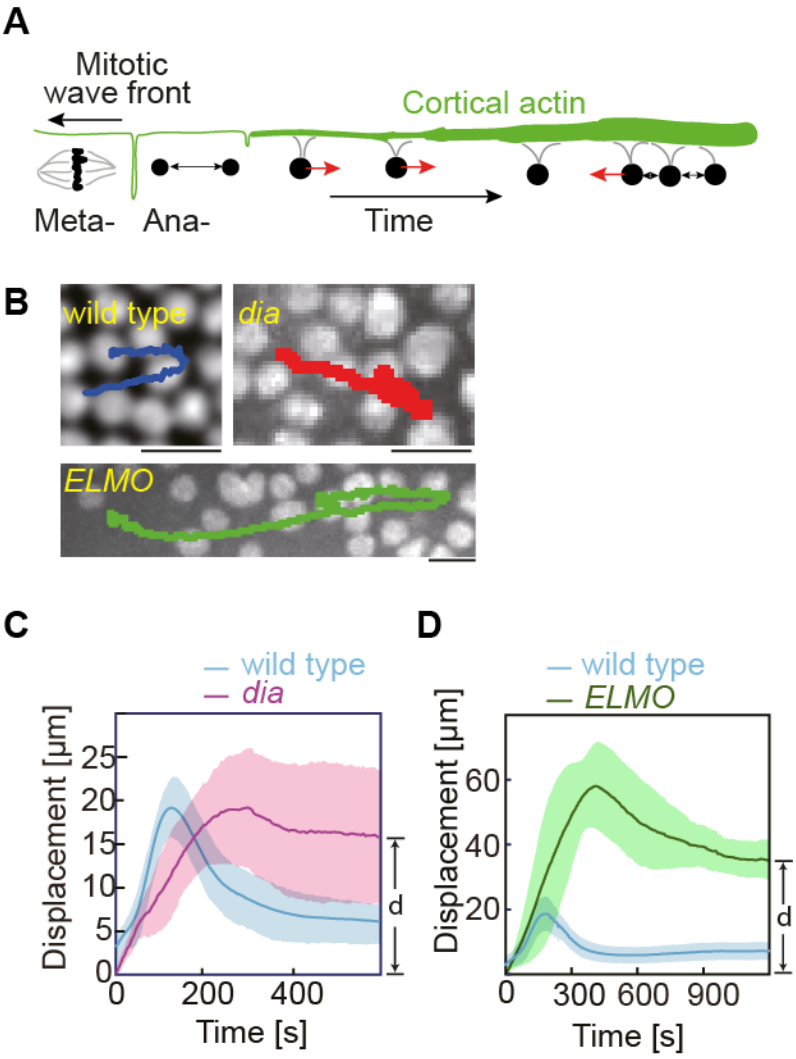

Figure 5. Role of the actin cortex. (A), Scheme of cortical actin dynamics during nuclear division cycles. (B), Images from movies of *dia* and *ELMO* mutants. Nuclear trajectories over 10 min are plotted into the last images. (C, D), Time course of displacement in *dia* and *ELMO* mutants. The Data are mean±s.e.m. Scale bar: 10 μm.

We also detected changes in nuclear movement in *dia* mutants. Similar to *ELMO* mutants, we observed a loss of the spring-like back movement. The nuclei did not return to their initial position and the spring constant was almost 10-fold reduced (Fig. 5D, Supp. Data Fig. S6D, E). In contrast to *ELMO*, the maximal displacement was similar to wild type indicating that the stabilizing/viscos function of the cortex does not depend on *dia*. The neighborhood relationships were largely maintained *dia* and *ELMO* embryos (Supp. Data Fig. S6F). In summary, by employing two mutants affecting F-actin organization, we identified distinct functions of the actin cortex. F-actin is required for the back movement as revealed by the reduced apparent spring constant and the permanent displacement. The *ELMO*-dependent organization into caps appears to be important for limiting nuclear movement.

Discussion

The direct interactions between the nuclei and their associated cytoskeleton are a special feature of syncytial embryos. Due to the lack of separating cell membranes, microtubule asters originating from the centrosomes associated with each nucleus form an extended network of hundreds to thousands of elements. Emergent features arise in this network by summing up the behavior of individual elements, such as fluctuations or duplication, and their interactions, such as repulsion. The analysis of the mechanism underlying the emergent features is essential for understanding how the individual cells function collectively to form a tissue.

We identified an anisotropic flow of the nuclear array as an emergent feature. Based on a morphodynamical analysis of the nuclear array in wild type and mutant embryos together with computational simulations, we analyzed the mechanism of the flow behavior. In this way we identified spindle elongation drives nuclei moving away whereas cortical F-actin restores the nuclear positions, which is necessary for the following development. The emergent nature of the nuclear flow becomes obvious, since individual behavior is strikingly different than the collective behavior of the nuclear array. Nuclei divide with an isotropic orientation, whereas the flow direction is anisotropic. Furthermore the maximal division distance is about 10 μm, whereas the maximal displacement is about 20 μm.

The mitotic pseudo-synchrony is necessary for the completion of nuclear division, especially in late cleavage cycle with high nuclear density. With the pseudo-synchrony comes the nuclear directional movement. With strongly synchronous divisions, the pushing forces of mitotic spindles would generate a spatially isotropic force distribution. Consequently, the nuclei would not move due to a balance in forces. However, in the case

of pseudo-synchronous divisions, the force balance is broken leading to an imbalance and thus a flow away from the wave front. The repulsive force between daughter nuclei increases in anaphase pushing the daughter nuclei apart, followed by a drop in telophase due to spindle disassembly (Supp. Data Fig. S7A). The summing up of all nuclei in an embryo at a given mitotic time results in an asymmetric force field, which likely determines the directionality of the nuclear flow in telophase (Supp. Data Fig. S7B).

Upon the nuclei reach the maximal displacements, they return to the starting positions. Consistency of nuclear position among different cleavage cycles is important for maintaining the positioning information provided by morphogens. We identified a contribution of the actin cortex to the viscoelastic feature of the nuclear movement, i.e. that nuclei return to their starting position. This is consistent with previous findings that the elasticity of *Drosophila* embryonic cortex in cellularization stage depends on the actin cytoskeleton (23, 24). In addition, the structure of actin cortex is undergoing remodeling, which may contribute to the returning movements by actively changing the cortical material properties in time and space.

Collective behaviors driven by the integration of forces originated from cytoskeletal networks are indispensable in biological systems. Some basic ingredients of the system — the mechanical properties of the cytoskeleton and the function of motor proteins have been well studied *in vitro*. The morphology of early *Drosophila* embryos has also been extensively imaged. However, the assembly of the puzzle to achieve a quantitative understanding of the molecular mechanics behind the dynamical self-organization of the rapidly developing embryo, has only begun to be explored. Our study of the dynamical properties of the syncytial embryo is a first step towards our long-term goal to understand how cells mechanically interact with each other and collectively function as active matter forming a tissue.

Methods and Materials

Drosophila Genetics

Fly stocks were obtained from the Bloomington Drosophila Stock Center (35, 36), unless otherwise noted. Fly strains used in this study are the followings: w; Histone2Av-GFP. *w*; sqh-Utr-GFP/CyO; ubi-His2Av-RFP(29). *Map60*^{KG00506}. *w*; ubi-GFP-D-Cad *dia*^{5} Frt^{2L} ubi-His2Av-RFP/CyO (32). *w* ; *ELMO*^{367} Frt^{2L}/CyO (21). *w Hira*^{ssm}/FM7c, w^{a} B (37). His2Av-RFP; Kinesin5-[TEV]-GFP (26). Fly stocks were kept at 25°C on a standard cornmeal food. Germline clones of *dia* and *ELMO* were induced by crossing with corresponding Frt chromosomes and the following heat shock at 37˚C for one hour on two consecutive days after hatching. Short spindle induced by TEV injection was described previously(26). In addition, we titrated the amount of TEV protease to achieve a partial depletion allowing mitosis but with shorter spindles during the cleavage cycle.

Phalloidin staining and imaging

Wild type embryos and embryos from *dia* and *ELMO* germline clones were fixed with 8% formaldehyde according to standard procedures. The vitelline membrane was manually removed. Fixed embryos were incubated with phalloidin-Alexa 488 (1:500, Thermo Fisher) for 1.5 h. After rinsing three times and washing three times for 15 min each with PBT (PBS(Phosphate-Buffered Saline) with 0.1% Tween 20), embryos were stained with DAPI (4′,6-Diamidine-2′-phenylindole dihydrochloride) (0.2 μg/ml) for 10 min, rinsed three times in PBT, washed in PBT for 10 min and mounted in Aqua-Poly/Mount (Polysciences). The images of fixed embryos were acquired using a Zeiss LSM780 confocal microscope.

Microinjection

1–2 h old embryos were collected, dechorionated with 50% bleach solution for 90 s, rinsed thoroughly with deionized water. After aligning on a coverslip, the embryos were desiccated for 10 min, and covered with halocarbon oil (Voltalef 10S, Lehmann & Voss). TEV protease (a gift from Dirk Görlich) and Histone1-Alexa-488 protein (2 mg/ml, Thermo Fisher) were injected to the desired embryos using Microinjector FemtoJet® (Eppendorf) on an inverted microscope.

Live imaging for nuclear dynamics

Nuclear dynamics was recorded by movies of embryos with the fluorescently labeled nuclei, by expression of Histone2Av-GFP or injection of Histone1-Alexa-488 protein. Embryos were attached on a coverslip coated with embryo glue and covered with halocarbon oil. Time-lapse images were recorded on a spinning disc microscope (Zeiss, 25x/NA0.7 multi immersion) with an emCCD camera (Photometrics, Evolve 512). To ensure reliable tracking of the nuclei, the frame rate was 0.5–0.2 Hz with 4 axial sections, covering 8 μm. Images were merged maximal intensity projections (Fiji/ImageJ(38)).

Images process and quantification

Imaging segmentation and analysis were performed with custom-written Python algorithms. The software code is available on request. Briefly, the nuclear positions were detected as blob-like features of size σ_i at position (x_i, y_i) by finding the maxima $(x_i, y_i\ \sigma_i)$ of a rescaled Laplacian of Gaussian (LoG) function

$$L(x, y, \sigma) = \sigma^2\big(\Delta(g_\sigma * f)\big)(x, y, \sigma),$$

where $f_t\,(x, y)$ is the nuclei gray-scale value at time t, $g_\sigma\,(x, y)$ is Gaussian kernel of width σ, and "$g * f$" stands for the convolution of function g and f. When multiple blobs were detected in a single nucleus, we deleted a neighboring blob b_2 of b_1 with a heuristic test function T

$$T(b_1\,, b_2) = \frac{1}{2\big(f_t(b_1) + f_t(b_2)\big)} - \int_r f_t(x) e^{-\left(x-\frac{1}{2}\right)^2} dx,$$

where $\gamma : [0, 1] \to \mathbb{R}^2$ is the straight line from b_1 of b_2.

We tracked the nuclei across frames based on a proximity criterion. The distance between nucleus k in frame i and l in frame $i+1$ was defined as

$$d_{k,l} = \| x_{k,i} - x_{l,i+1} \|_2.$$

We determined the interval of mitosis time using the k-means-clustering algorithm on the observed nucleus positions at time t. If a new blob was detected, we considered this nucleus and its nearest neighbor were daughter nuclei from a recent mitosis, and set their internal nucleus clock to 0. Calculations of nuclear displacement, speed, nuclear density, spindle length and orientation were done for each nucleus in its own eigentime after mitosis.

Quantification of F-actin over cell cycle

Embryos expressing Histone2Av-RFP; Utrophin-GFP were imaged with a Zeiss LSM780 confocal microscope (25x/NA0.7 multi immersion). The frame rate was 0.1 Hz, and 10 μm was covered in z direction. Utrophin-GFP stacks were merged by average intensity projection (Fiji/ImageJ). F-actin was quantified manually with Fiji/ImageJ.

2D simulation of synchronous mitosis

In the simulation, the nuclei are randomly placed in a 50um*50um square via Poisson-disc sampling, which produces random tightly-packed locations with pair-wise distances not smaller than a specified value d_{disc}>4um. We assume the nuclei divide simultaneously and form mitotic spindles with isotropic orientations. As the spindles extend with a constant speed, we check at each time step if any two of the spindles touch each other by scanning a restricted area of 4um*4um in the vicinity of each spindle (see supplementary video). If a spindle touches at least one other, we assume it stops extending and reaches its maximal length due to limited space. When all spindles reach their respective maximal lengths, the simulation is ended and we compute the average maximal length l_{max} over all spindles in the simulation. For each fixed d_{disc}, we run the simulation 50 times, producing 50 l_{max} values for various nuclear density around $1/(4d_{disc}^2)$. The mean of the 50 l_{max} values and the mean of the 50 nuclear densities provide the coordinates of one point in Fig.1C. The x- and y- error bars indicate the respective standard deviations. Varying the minimum distance d_{disc} between nuclei, we obtain the mean l_{max} values for a range of nuclear densities. The data from simulation are fitted to a power-law function (solid curve in Fig.1C) with the method of least squares.

Computational modeling of the nuclear movement

We base our model on a previously successful model for static nuclei packing during interphase[4]: Nuclei, positioned at $\vec{r}_i$, move due to active forces, $\vec{F}_{act,ij}$, exerted by motor-activated pushing apart of neighbouring overlapping microtubule asters and due to passive repulsive forces between neighbouring nuclei, $\vec{F}_{pass,ij}$,arising from the visco-elastic matrix embedding nuclei, mainly build by actin cytoskeletal elements. The overdamped equation of

motion is given by $r_i = \frac{1}{\eta}\sum_{j\neq i}\left(\vec{F}_{act,ij} + \vec{F}_{pass,ij}\right)$, where η denotes the viscosity of the matrix. Aiming to describe the motion of nuclei during mitosis we adjust force amplitudes to change as microtubuli and actin cortex of nuclei considered remodels over time, $\vec{F}_{pass,ij} = -A_{pass}(t_i)A_{pass}(t_j)\frac{\vec{e}_{r_{i,j}}}{r_{i,j}^4}$, $\vec{F}_{act,ij} = -A_{act}(t_i)A_{act}(t_j)\frac{\vec{e}_{r_{i,j}}}{r_{i,j}^4}$, where $\vec{e}_{r_{i,j}}$ and $r_{i,j}$ denote the unit vector and the distance between nuclei i,j considered. Individual nuclei times t_i are shifted with respect to nuclei division at $t_{\text{div}} = 0$. To capture the dynamics of cytoskeletal elements during mitosis we subdivided the time course of events into the series: $t_{\text{spindle ass}} < t_{\text{spindle const}} < t_{\text{div}} < t_{\text{div max}} < t_{\text{sp diss}} < t_{\text{MT ass}} < t_{\text{actin ass}} < t_{\text{MT inter}} < t_{\text{actin inter}}$. Passive forces change only between $t_{\text{spindle ass}} < t_{\text{spindle const}}$ when actin caps shrink while spindles assemble to generate balancing forces and during regrowth of actin caps between $t_{\text{actin ass}} < t_{\text{actin inter}}$ before entering interphase. Active forces due to spindle formation as well as microtubule asters are in contrast much more dynamic. Between $t_{\text{spindle ass}} < t_{\text{spindle const}}$ spindles assemble. Upon division $t_{\text{div}} < t_{\text{spindle diss}}$ spindles move daughter nuclei apart, active force between only the division partners is now increased by an additional time-dependent factor A_{div} that reaches a value of up to 3. Afterwards, forces between paired daughter nuclei reduce linearly to regular levels. Meanwhile, for all other nuclei, after division the active force is halved due to distribution of centrosomes on two nuclei. This is balanced by the effective increase of passive forces as nuclei are closer packed due to division while the passive force amplitude stays constant. Between $t_{\text{spindle diss}} < t_{\text{MT ass}}$ spindles disassemble before the microtubule asters regrow during $t_{\text{MT ass}} < t_{\text{MT inter}}$. All dynamics are interpolated linearly. In detail:

$$A_{\text{pass}}(t) = \begin{cases} h_{\text{inter}} & t \leq t_{\text{spindle ass}} \\ h_{\text{inter}} + (h_{\text{mitosis}} - h_{\text{inter}})\frac{t - t_{\text{spindle ass}}}{t_{\text{spindle const}} - t_{\text{spindle ass}}} & t_{\text{spindle ass}} \leq t \leq t_{\text{spindle const}} \\ h_{\text{mitosis}} & t_{\text{spindle const}} \leq t \leq t_{\text{actin ass}} \\ h_{\text{mitosis}} + (h_{\text{inter}} - h_{\text{mitosis}})\frac{t - t_{\text{actin ass}}}{t_{\text{actin inter}} - t_{\text{actin ass}}} & t_{\text{actin ass}} \leq t \leq t_{\text{actin inter}} \\ h_{\text{inter}} & t_{\text{actin inter}} \leq t \end{cases},$$

$$A_{\text{act}}(t) = \begin{cases} h_{\text{MT}} & t \leq t_{\text{spindle ass}} \\ h_{\text{MT}} + \left(h_{\text{sp}} - h_{\text{MT}}\right)\frac{t - t_{\text{spindle ass}}}{t_{\text{spindle const}} - t_{\text{spindle ass}}} & t_{\text{spindle ass}} \leq t \leq t_{\text{spindle const}} \\ h_{\text{spindle}} & t_{\text{spindle const}} \leq t \leq t_{\text{div}} \\ \frac{1}{2}h_{\text{spindle}} & t_{\text{div}} \leq t \leq t_{\text{spindle diss}} \\ \frac{1}{2}h_{\text{spindle}} + \frac{1}{2}\left(h_{\text{spindle diss}} - h_{\text{spindle}}\right)\frac{t - t_{\text{spindle diss}}}{t_{\text{MT ass}} - t_{\text{spindle diss}}} & t_{\text{spindle diss}} \leq t \leq t_{\text{MT ass}} \\ \frac{1}{2}h_{\text{spindle diss}} + \frac{1}{2}\left(h_{\text{MT}} - h_{\text{spindle diss}}\right)\frac{t - t_{\text{MT ass}}}{t_{\text{MT inter}} - t_{\text{MT ass}}} & t_{\text{MT ass}} \leq t \leq t_{\text{MT inter}} \\ \frac{1}{2}h_{\text{MT}} & t_{\text{MT inter}} \leq t \end{cases},$$

$$A_{\text{div}}(t) = \begin{cases} h_{\text{div}} \dfrac{t - t_{\text{div}}}{t_{\text{spindle diss}}/2 - t_{\text{div}}} & t_{\text{div}} \leq t \leq t_{\text{spindle diss}}/2 \\ h_{\text{div}} & t_{\text{spindle diss}}/2 \leq t \leq t_{\text{spindle diss}} \\ h_{\text{div}} - (h_{\text{div}} - 1) \dfrac{t - t_{\text{spindle diss}}}{t_{\text{MT ass}} - t_{\text{spindle diss}}} & t_{\text{spindle diss}} \leq t \leq t_{\text{MT ass}} \\ 1 & t_{\text{MT ass}} \leq t \end{cases}$$

Note that changes in both passive and active forces only get out of balance during spindle disassembly initiating nuclei motion with significant time delay relative to the time point of nuclei division. At that point in time nuclei that have not divided yet have a stronger repulsive force than the already divided nuclei due both actin caps and microtubule asters not yet being fully formed. Therefore, nuclei move toward the region of higher nuclei density, only returning back when actin caps and microtubule asters are forming again.

Nuclei dynamics are evolved on a sphere to capture the topology of the embryo. Division wave is initiated on one pole and propagates with velocity v toward the opposing pole. For numerical stability we place two daughter nuclei upon division a short distance r at a random angle apart, their center of mass coincides with the position of their mothers.

Spring constant fitting

The data sets consisted of 1–5 nuclear displacement curves for 2–4 embryos of each type (*dia*, *ELMO*, *Kinesin5* and *Map60* mutants, wild type).
The nuclear displacement curves (in the first phase) are similar to the oscillation of a not-actively driven and non-damped harmonic oscillator. Therefore, the individual nuclear displacement curves were fitted to a sine curve of the form $y(t) = A \sin(\omega t + \varphi)$, where A is the amplitude, ω the angular frequency and φ the phase shift, using a self-written script in Python. The biological rational behind this approach is that the nuclei behave like they were linked to an elastic spring, which could be e.g. linkages to the cytoskeleton. At t=0 the spring is stretched and the nuclei start to move until the spring is compressed and the nuclei move back.

The fit region was determined as follows. For all curves, the lower bound on the fitting range was set equal to the point in time where the nuclear displacement first exceeds 5 µm, as some curves show a small, reversible displacement in the beginning. The upper bound was chosen independently for each of the data sets since the elastic part of the curve depends on the stiffness and dampening of the spring and hence differs across data sets. For the *dia* and *Map60* mutants as well as the wild type, the upper bound was set equal to 100 s after the turning point, while it was set to 180 s after for the *ELMO* mutant and 240 s for the Kinesin5 mutants. The results of the fit parameter ω were averaged for each embryo to give a set of angular frequencies ω_i for each type, where i runs over the number of embryos. The spring constant was derived from the average ω_i *via* the relation

$k = m\,(\omega_i)^2$,in which m denotes the mass of the nucleus. It was assumed that the nuclei are spherical with a diameter of 4.9 μm and a density equal to that of water at room temperature. Error bars, which correspond to one standard deviation, were calculated in the frequency domain and then converted to the force domain by the analogue of the relation above.

Acknowledgements
We are grateful to D. Görlich, T. Lecuit, B. Loppin and the members of the Grosshans laboratory for stains, materials and discussions. We acknowledge service support from the Bloomington Drosophila Stock Center (supported by NIH P40OD018537). X.Z. was supported by Center for Advancing Electronics Dresden (cfaed) and by the Deutsche Forschungsgemeinschaft (DFG, German Research Foundation) under Germany's Excellence Strategy – EXC-2068 – 390729961– Cluster of Excellence Physics of Life of TU Dresden. This work was in part supported by the Göttingen Centre for Molecular Biology (funds for equipment repair) and the Deutsche Forschungsgemeinschaft (DFG, SFB-937/A10, SFB-937/A19 and equipment grant INST1525/16-1 FUGG).

Author contributions
ZL conducted the experiments. ZL, JR, HP, SK analyzed the data. SM, XZ, KA conducted the simulations. JG and ZL conceived and JG, TA, SG, KA supervised the study. JG, ZL and XZ wrote the manuscript.

References

1. Couzin ID (2018) Synchronization: The Key to Effective Communication in Animal Collectives. *Trends in Cognitive Sciences* 22(10):844–846.

2. Partridge BL (1982) Rigid definitions of schooling behaviour are inadequate. *Animal Behaviour* 30(1):298–299.

3. Moussaid M, Garnier S, Theraulaz G, Helbing D (2009) Collective Information Processing and Pattern Formation in Swarms, Flocks, and Crowds. *Topics in Cognitive Science* 1(3):469–497.

4. Chialvo DR (2010) Emergent complex neural dynamics. *Nature Physics* 6(10):744–750.

5. Levina A, Herrmann JM, Geisel T (2007) Dynamical synapses causing self-organized criticality in neural networks. *Nature Physics* 3(12):857–860.

6. Plenz D, Thiagarajan TC (2007) The organizing principles of neuronal avalanches: cell assemblies in the cortex? *Trends in Neurosciences* 30(3):101–110.

7. McMahon A, Supatto W, Fraser SE, Stathopoulos A (2008) Dynamic Analyses of

Drosophila Gastrulation Provide Insights into Collective Cell Migration. *Science* 322(5907):1546–1550.

8. Farrell JA, et al. (2018) Single-cell reconstruction of developmental trajectories during zebrafish embryogenesis. *Science* 360(6392):eaar3131.

9. Sumino Y, et al. (2012) Large-scale vortex lattice emerging from collectively moving microtubules. *Nature* 483(7390):448–452.

10. Schaller V, Weber C, Semmrich C, Frey E, Bausch AR (2010) Polar patterns of driven filaments. *Nature* 467(7311):73–77.

11. Butt T, et al. (2010) Myosin motors drive long range alignment of actin filaments. *J Biol Chem* 285(7):4964–4974.

12. Deneke VE, Melbinger A, Vergassola M, Di Talia S (2016) Waves of Cdk1 Activity in S Phase Synchronize the Cell Cycle in Drosophila Embryos. *Developmental Cell* 38(4):399–412.

13. Idema T, et al. (2013) The Syncytial Drosophila Embryo as a Mechanically Excitable Medium. *PLoS ONE* 8(10):e77216.

14. Kanesaki T, Edwards CM, Schwarz US, Grosshans J (2011) Dynamic ordering of nuclei in syncytial embryos: a quantitative analysis of the role of cytoskeletal networks. *Integr Biol (Camb)* 3(11):1112–1119.

15. Kaiser F, et al. (2018) Mechanical Model of Nuclei Ordering in Drosophila Embryos Reveals Dilution of Stochastic Forces. *Biophys J* 114(7):1730–1740.

16. Quinlan ME (2016) Cytoplasmic Streaming in the Drosophila Oocyte. *https://doiorg/101146/annurev-cellbio-111315-125416* 32(1):173–195.

17. Woodhouse FG, Goldstein RE (2013) Cytoplasmic streaming in plant cells emerges naturally by microfilament self-organization. *PNAS* 110(35):14132–14137.

18. Shimmen T, Yokota E (2004) Cytoplasmic streaming in plants. *Current Opinion in Cell Biology* 16(1):68–72.

19. Deneke VE, et al. (2019) Self-Organized Nuclear Positioning Synchronizes the Cell Cycle in Drosophila Embryos. *Cell*. doi:10.1016/j.cell.2019.03.007.

20. He B, Doubrovinski K, Polyakov O, Wieschaus E (2014) Apical constriction drives tissue-scale hydrodynamic flow to mediate cell elongation. *Nature* 508(7496):392–396.

21. Winkler F, et al. (2015) Fluctuation Analysis of Centrosomes Reveals a Cortical

Function of Kinesin-1. *Biophys J* 109(5):856–868.

22. Wessel AD, Gumalla M, Grosshans J, Schmidt CF (2015) The mechanical properties of early Drosophila embryos measured by high-speed video microrheology. *Biophys J* 108(8):1899–1907.

23. Doubrovinski K, Swan M, Polyakov O, Wieschaus EF (2017) Measurement of cortical elasticity in Drosophila melanogaster embryos using ferrofluids. *Proc Natl Acad Sci USA* 114(5):1051–1056.

24. D'Angelo A, Dierkes K, Carolis C, Salbreux G, Solon J (2019) In Vivo Force Application Reveals a Fast Tissue Softening and External Friction Increase during Early Embryogenesis. *Current Biology* 29(9):1564–1571.e6.

25. Scholey JM (2009) Kinesin-5 in Drosophila embryo mitosis: Sliding filament or spindle matrix mechanism? *Cell Motility and the Cytoskeleton* 66(8):500–508.

26. Lv Z, Rosenbaum J, Aspelmeier T, Grosshans J (2018) A "molecular guillotine" reveals an interphase function of Kinesin-5. *J Cell Sci*:jcs.210583.

27. Sullivan W, Theurkauf WE (1995) The cytoskeleton and morphogenesis of the early Drosophila embryo. *Current Opinion in Cell Biology* 7(1):18–22.

28. Karr TL, Alberts BM (1986) Organization of the cytoskeleton in early Drosophila embryos. *The Journal of Cell Biology* 102(4):1494–1509.

29. Rauzi M, Lenne P-F, Lecuit T (2010) Planar polarized actomyosin contractile flows control epithelial junction remodelling. *Nature* 468(7327):1110–1114.

30. Schmidt A, Lv Z, Grosshans J (2018) ELMO and Sponge specify subapical restriction of Canoe and formation of the subapical domain in earlyDrosophilaembryos. *Development* 145(2):dev157909.

31. Geisbrecht ER, et al. (2008) Drosophila ELMO/CED-12 interacts with Myoblast city to direct myoblast fusion and ommatidial organization. *Dev Biol* 314(1):137–149.

32. Afshar K, Stuart B, Wasserman SA (2000) Functional analysis of the Drosophila diaphanous FH protein in early embryonic development. *Development* 127(9):1887–1897.

33. Grosshans J, et al. (2005) RhoGEF2 and the formin Dia control the formation of the furrow canal by directed actin assembly during Drosophila cellularisation. *Development* 132(5):1009–1020.

34. Wenzl C, Yan S, Laupsien P, Grosshans J (2010) Localization of RhoGEF2 during Drosophila cellularization is developmentally controlled by Slam. *Mech Dev* 127(7-

8):371–384.

35. Gramates LS, et al. (2017) FlyBase at 25: looking to the future. *Nucleic Acids Res* 45(D1):D663–D671.

36. Cook KR, Parks AL, Jacobus LM, Kaufman TC, Matthews K (2010) New research resources at the Bloomington Drosophila Stock Center. *Fly* 4(1):88–91.

37. Loppin B, Docquier M, Bonneton F, Couble P (2000) The Maternal Effect Mutation sésame Affects the Formation of the Male Pronucleus in Drosophila melanogaster. *Dev Biol* 222(2):392–404.

38. Schindelin J, et al. (2012) Fiji: an open-source platform for biological-image analysis. *Nat Methods* 9(7):676–682.

Figure S1. Nuclear densities in different cycles. a, images of Drosophila syncytial embryo expressing Histone2Av-GFP in different cycles. **b**, quantification of nuclear density in the indicated cycles. n=10 embryos. Data are mean±s.e.m.

Figure S2. Asynchronous nuclear division. (A), Embryo to embryo variation of the speed of the wave front (n=50 embryos). (B) The protected area between daughter nuclei containing the spindle is indicated by an overlaid colored area. (C), Illustration of the simulation used in Fig. 1B. Daughter nuclei (arrow heads) are symmetrically pushed apart until they reach a neighboring arrow (red dot). Mother nucleus (green).

Figure S3. Image analysis pipeline and the quantification of nuclear dynamics. (A), The live images of the embryos with labelled nuclei were taken with a frame rate of 0.2 Hz. Nuclei were detected and tracked using custom-written Python algorithms. (B), Time course of nuclear displacement, with colour-coding for individual nuclei (n=10 nuclei). (C), Time course of nuclear flow speed, with colour-coding for individual embryos (n=10 embryos). (D), The distribution of angles of spindle and nuclear flow, with colour-coding for individual embryos (n=20 embryos). n>50 nuclei in each embryo in figure C and D.

Figure S4. Nuclear displacement and flow speeds are less pronounced in earlier cycles. a, The time course of nuclear displacement in NC11, 12 and 13 in one embryo (n=58, 107 and 206 nuclei in NC11, 12 and 13, respectively). **b**, Maximal displacement distribution in NC11, 12 and 13 from **a**. **c**, Time course of nuclear flow speed from the same embryo as shown in a, with colour-coding for indicated nuclear cycles. **d**, The percentage of embryos showing the nuclear flow in different cycles (n=6, 18, 26 embryos in NC11, 12 and 13, respectively). Data are mean±s.e.m.

Figure S5. Numerical simulation used in Fig. 4. (A), Scheme of division, active and passive forces in syncytial embryo. (B), Time course of the division, active force and passive force used in the simulation. (C), Snap shots from the simulation. Nuclei were projections. Color code indicates speed of nuclear movement. (D), Increasing in spindle strength ($h_{spindle}$) leads to increasing of maximal displacement and division distance. Data are mean±s.e.m.

Figure S6. Actin cortex represses nuclear movement. (A), Live-images showing F-actin organization during nuclear cycle. (B), Quantification of F-actin. (n=10 regions in 3 independent recordings). (C), ELMO and Dia are involved in F-actin cortex formation. Fixed *dia* and *ELMO* mutants stained for F-actin (red) and DNA (blue). (D), Maximal displacement and final distance of nuclear dynamics in *dia* and *ELMO* mutants. (E), Apparent spring constant. (F), Neighborhood relationship. Images from movies at indicated time. Groups of cells have been marked in color at metaphase. Their daughter nuclei were labelled with the same color in the following images. (G), Images from movies of wild type and *ELMO* mutants in NC12. Nuclear trajectories are plotted into the first images. (H), The time course

of nuclear displacement in NC12. (n=130 nuclei in *ELMO* and 290 nuclei in wild type. Data are mean±s.e.m. Scale bar: 10 μm.

Figure S7. The asymmetric force field leads to the nuclear directional movement. (A), The repulsive force between daughter nuclei increases in anaphase pushing the daughter nuclei apart, followed by a drop in telophase due to spindle disassembly. (B), The summing up of all nuclei in an embryo at a given mitotic time results in an asymmetric force field, which likely determines the directionality of the nuclear flow in telophase.

Movie list:

Movie 1. Mitotic wave sweeps over the embryo.

Movie 2. Nuclei undergo stereotypical movement after metaphase-anaphase transition. Scale bar: 10 μm.

Movie 3. The time course of the nuclear Voronoi map over nuclear division. Scale bar: 10 μm.

Movie 4. Computational simulation.

Movie 5. The nuclear displacement in wild type, dia and ELMO mutant embryos. Scale bar: 20 μm.

Figure S1.

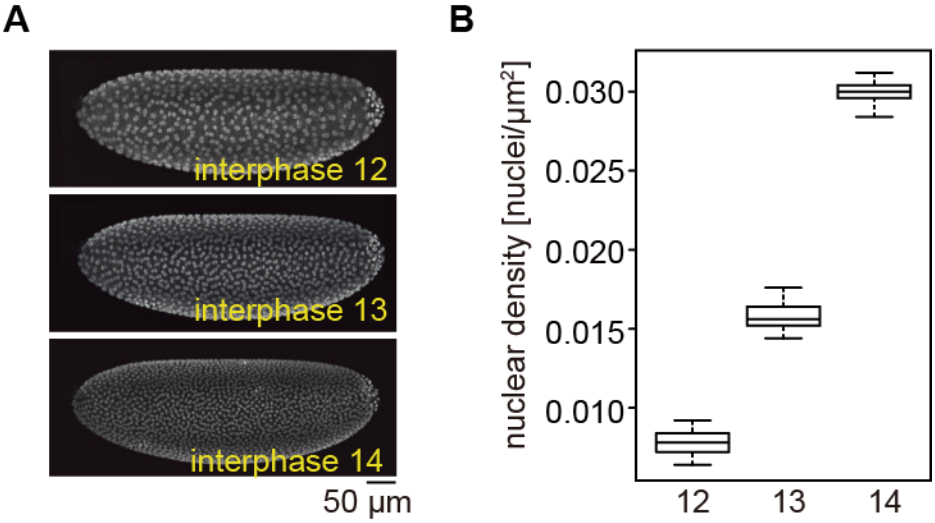
A
interphase 12
interphase 13
interphase 14
50 µm
B
nuclear density [nuclei/µm²]
0.030
0.025
0.020
0.015
0.010
12
13
14

Figure S2.

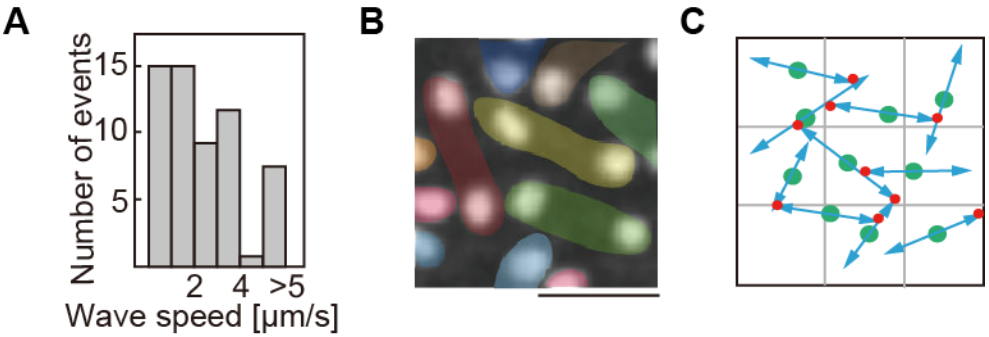

Figure S3.

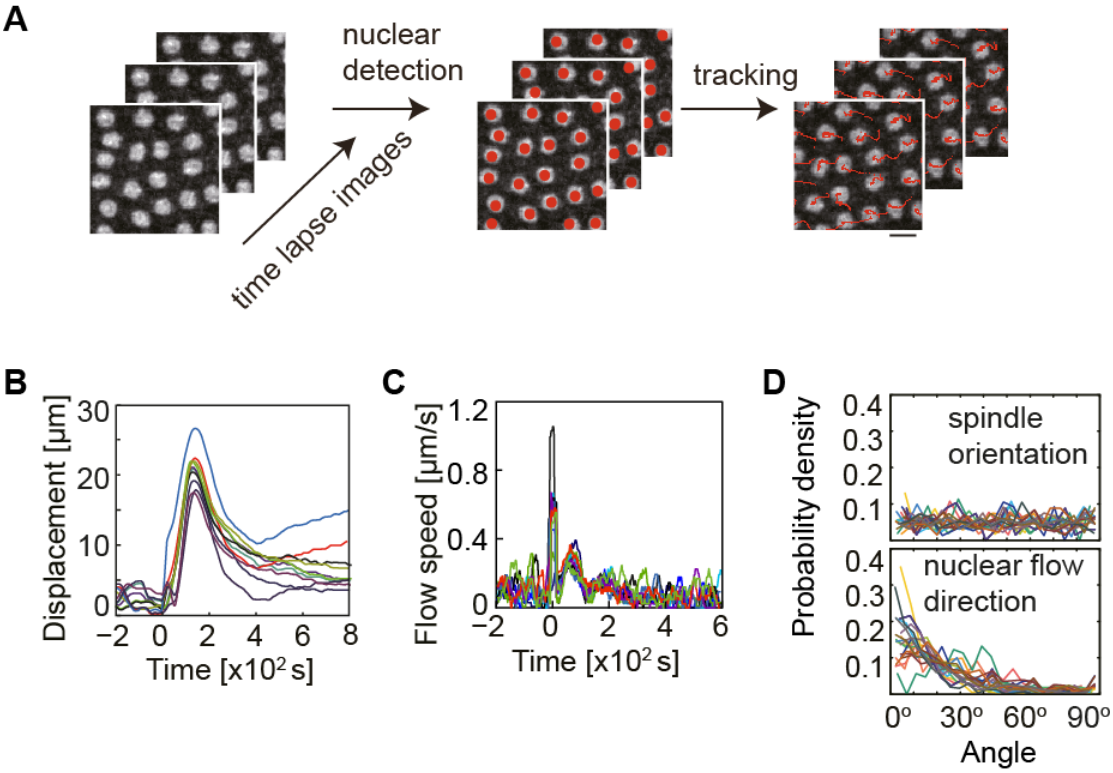
A
nuclear
detection
tracking
time lapse images
B
Displacement [μm]
30
20
10
0
−2 0 2 4 6 8
Time [x10² s]
C
Flow speed [μm/s]
1.2
0.8
0.4
0
−2 0 2 4 6
Time [x10² s]
D
Probability density
0.4
0.3
0.2
0.1
spindle
orientation
nuclear flow
direction
0° 30° 60° 90°
Angle

Figure S4.

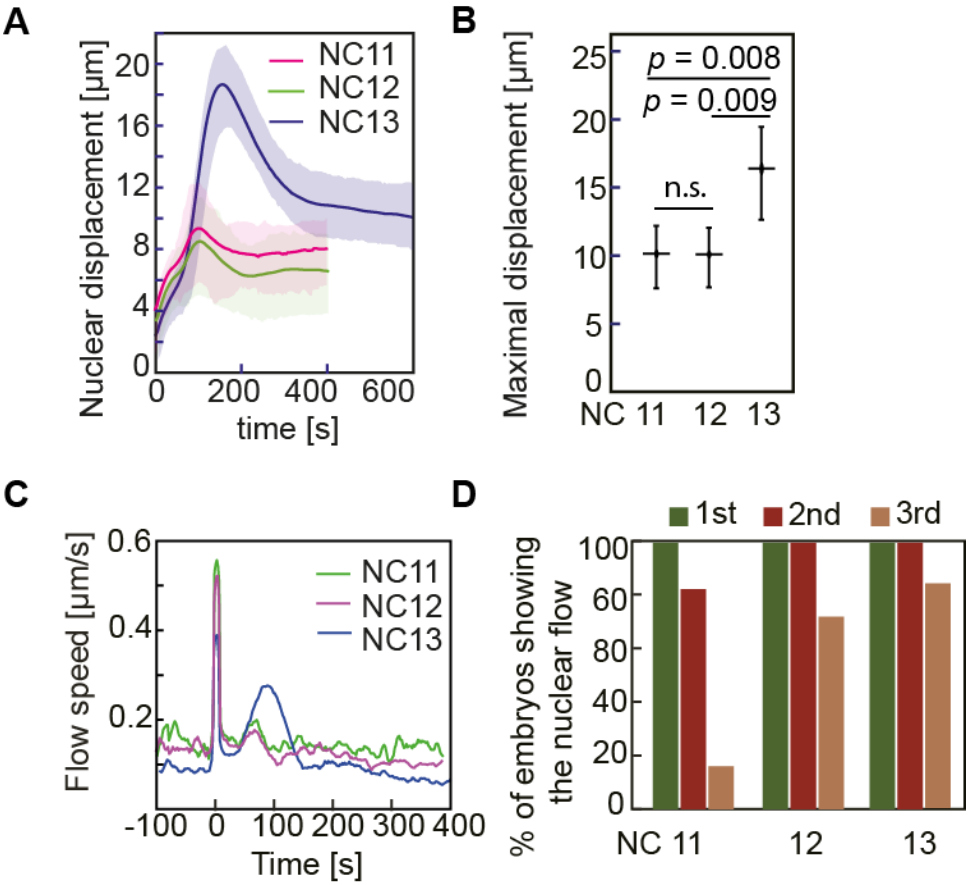
A
Nuclear displacement [μm]
20
16
12
8
4
0
0
200
400
600
time [s]
NC11
NC12
NC13
B
Maximal displacement [μm]
25
20
15
10
5
0
p = 0.008
p = 0.009
n.s.
NC 11
12
13
C
Flow speed [μm/s]
0.6
0.4
0.2
-100
0
100
200
300
400
Time [s]
NC11
NC12
NC13
D
1st
2nd
3rd
% of embryos showing the nuclear flow
100
60
80
40
20
0
NC 11
12
13

Figure S5.

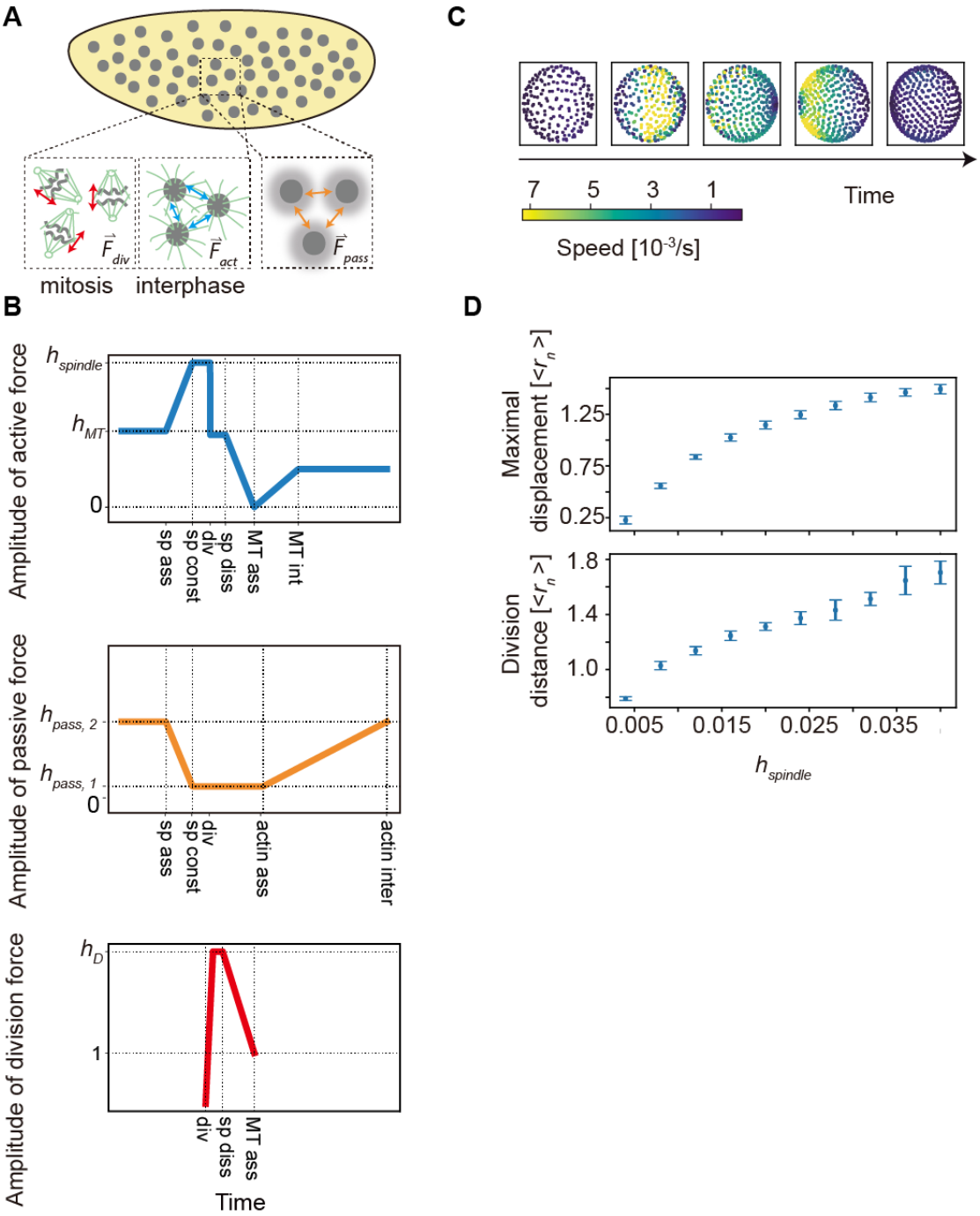
A
mitosis
interphase
B
Amplitude of active force
Amplitude of passive force
Amplitude of division force
Time
C
Time
Speed [10-3/s]
D
Maximal displacement [<rn>]
Division distance [<rn>]
hspindle

Figure S6.

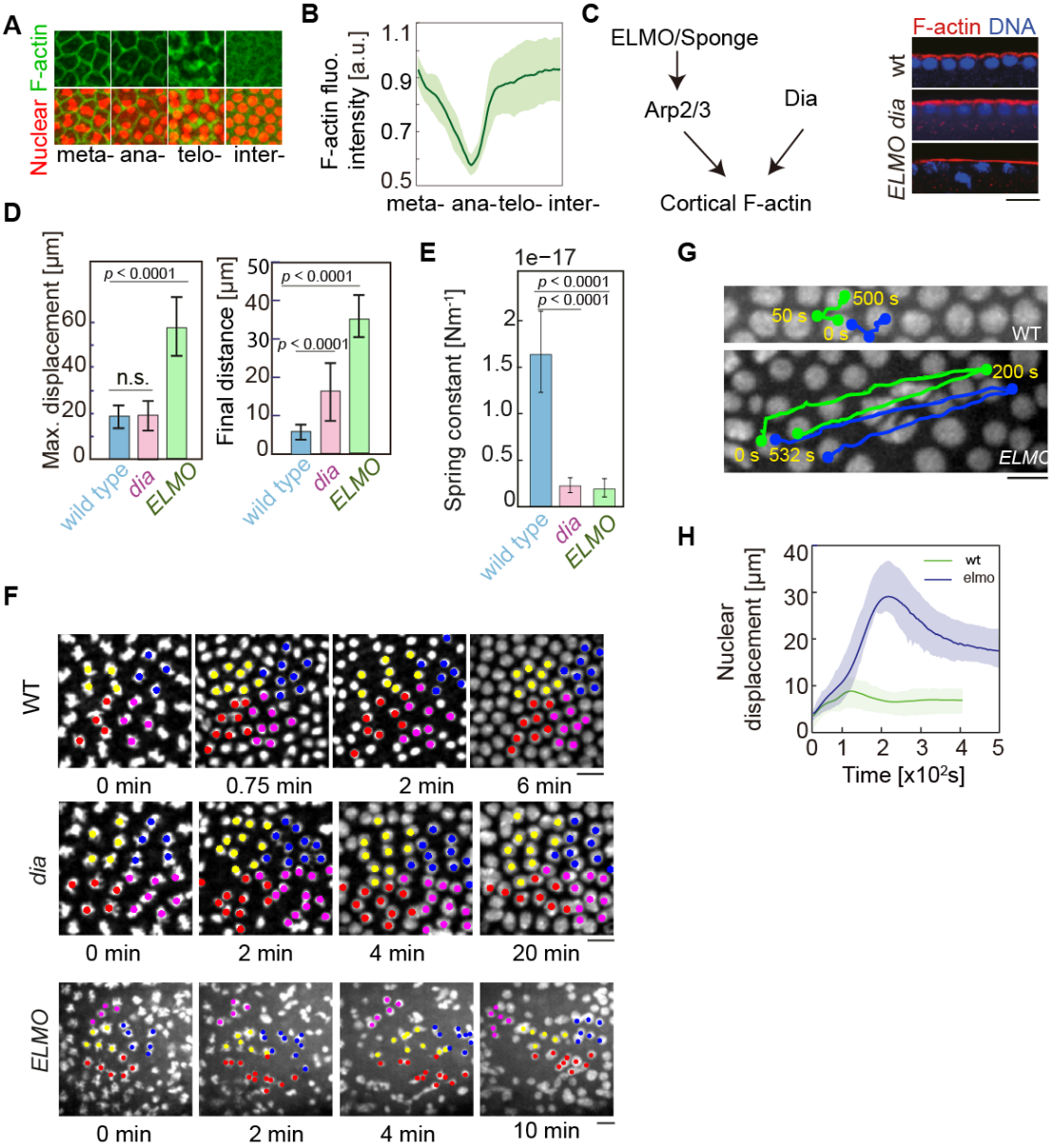
A
F-actin
Nuclear
meta- ana- telo- inter-
B
F-actin fluo. intensity [a.u.]
1.1
0.9
0.7
0.5
meta- ana- telo- inter-
C
ELMO/Sponge
Arp2/3
Dia
Cortical F-actin
F-actin DNA
wt
ELMO dia
D
Max. displacement [µm]
p < 0.0001
n.s.
wild type
dia
ELMO
Final distance [µm]
p < 0.0001
p < 0.0001
E
1e−17
Spring constant [Nm⁻¹]
p < 0.0001
p < 0.0001
G
500 s
50 s
0 s
WT
200 s
0 s
532 s
ELMO
H
Nuclear displacement [µm]
wt
elmo
Time [x10²s]
F
WT
0 min
0.75 min
2 min
6 min
dia
0 min
2 min
4 min
20 min
ELMO
0 min
2 min
4 min
10 min

Figure S7

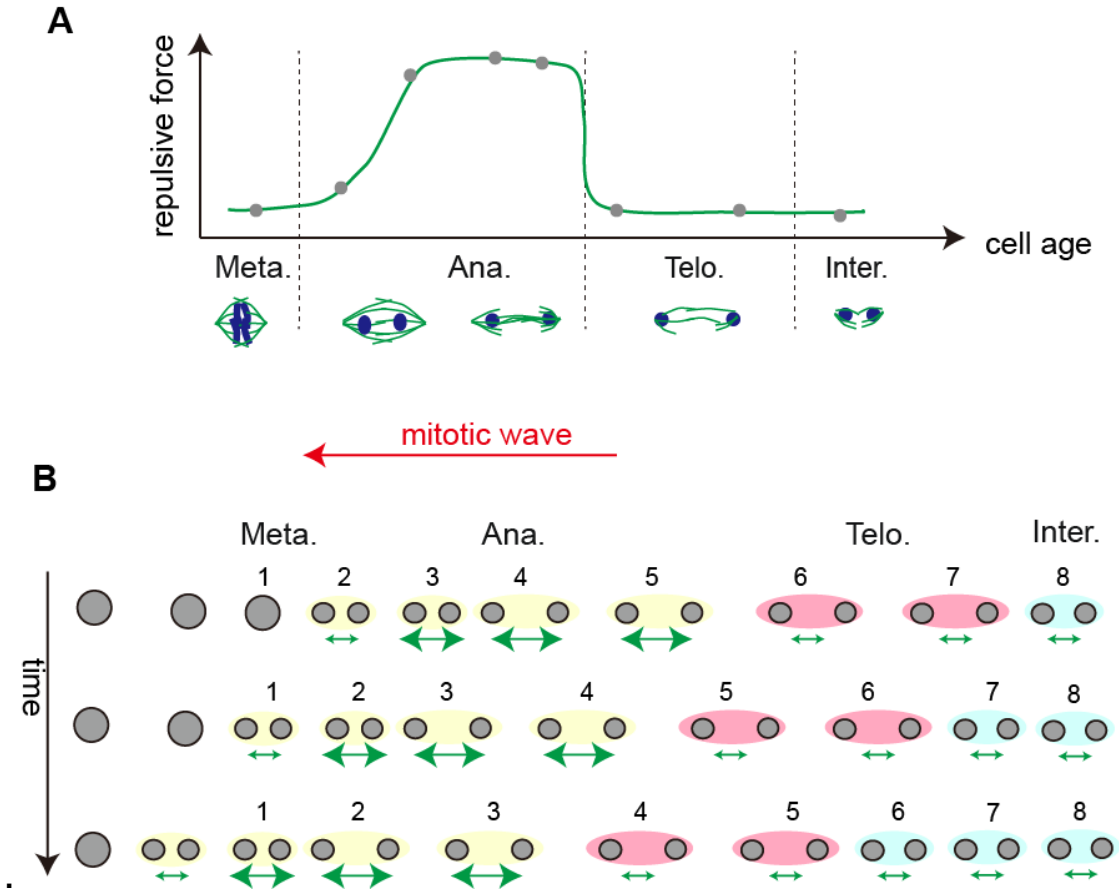
A
repulsive force
cell age
Meta.
Ana.
Telo.
Inter.
mitotic wave
B
Meta.
Ana.
Telo.
Inter.
time
1
2
3
4
5
6
7
8